arXiv:1603.00665v2 [cond-mat.mtrl-sci] 29 Sep 2016

Ab Initio Cycloidal and Chiral Magnetoelectric Responses in Cr_2O_3

Natalie Tillack* and Jonathan R. Yates
Department of Materials, University of Oxford, Oxford, OX1 3PH, United Kingdom

Paolo G. Radaelli
Department of Physics, University of Oxford, Oxford, OX1 3PU, United Kingdom

(Dated: September 30, 2016)

We present a thorough density functional theory study of the magneto-electric (ME) effect in Cr_2O_3. The spin-lattice ME tensor α was determined in the low-field and spin flop (SF) phases, using the method of dynamical magnetic charges, and found to be the sum of three distinct components. Two of them, a large relativistic "cycloidal" term and a small longitudinal term, are independent on the spin orientation. The third, only active in the SF phases is also of relativistic origin and arises from magnetic-field-induced chirality, leading to a non-toroidal ME response.

PACS numbers: 75.85.+t, 71.15.Rf, 75.30.Et, 75.30.Cr, 71.15.Mb

The search for magneto-electric (ME) materials, in which the electrical polarisation P (the magnetisation M) responds to the application of an external magnetic field H (electric field ϵ), has received a lot of attention in recent years [1–4], particularly in the context of 'modern' multiferroic materials with a spontaneous polarisation [5]. The linear magneto-electric effect, whereby P is linearly proportional to H, is also of current technological interest for magnetic storage devices, replacements of SQUIDs, and the ME switching of exchange bias [6–8]. In the 1950s, Landau and Lifshitz were the first to demonstrate that the ME effect only occurs in magnetic (*i.e.*, time-reversal odd) materials [9]. Cr_2O_3, often considered the prototypical ME, crystallises in the trigonal corundum structure and, below the Nèel temperature of $T_N = 307\,\mathrm{K}$, orders as a collinear antiferromagnet (AFM) with spins along the rhombohedral [111] direction (Fig. 1). Cr_2O_3 was predicted to be magneto-electric based on symmetry considerations [10, 11] — a prediction that was later verified experimentally [12–16]. Unlike most other MEs, Cr_2O_3 is ME above room temperature, making it technologically relevant in spite of the small ME response [17]. Cr_2O_3 is also ideal for studying the fundamental ME mechanisms, since it is not multiferroic, and – because of its magnetic point group – exhibits neither higher-order ME coupling nor piezomagnetism. Nevertheless, there is still a surprising amount of uncertainty surrounding the ME effect in Cr_2O_3, and in particular its behaviour throughout the T-H phase diagram; in turns this hampers the systematic search for materials with a stronger ME response.

The linear ME coupling can be described by an axial tensor of rank two:

$$\alpha_{ij} = \left(\frac{\partial P_i}{\partial H_j}\right) = \mu_0 \left(\frac{\partial M_j}{\partial \epsilon_i}\right) \qquad (1)$$

with $\mathbf{P}$ ($\mathbf{M}$) being the induced polarisation (magnetisation), $\mathbf{H}$ ($\boldsymbol{\epsilon}$) the external magnetic (electric) field, and μ_0 the magnetic permittivity. The components of P and H are conventionally expressed in a Cartesian coordinate system, with z along the rhombohedral [111] direction, x along one of the 2-fold axes, and y completing the right-handed set. The form of the linear ME tensor α_{ij} can be predicted entirely by symmetry once the AFM point group is known [18, 19]. In low applied H (LF phase), the Cr_2O_3 spins are aligned along z due to magnetic anisotropy [20, 21] (magnetic point group $\bar{3}'m'$), making α_{ij} diagonal and α_{11} and α_{22} being equal (Fig. 2). α_{33} is very small in the ground state, but becomes the dominant element at room temperature [22, 23]. Under strong applied fields along z, Cr_2O_3 undergoes a first-order phase transition into the so-called *spin flop* (SF) phase, with spins ordered in the same G-type pattern, but directed in the basal plane [24] (middle panel in Fig. 1). The possible magnetic point groups of the SF phase, $2'/m$, $2/m'$, or $\bar{1}'$ for spins *parallel* or *perpendicular* to x or in a generic direction, respectively, also allow for the ME effect, but with a different, off-diagonal form of the ME tensor (see Fig. 2), which is indeed observed experimentally [25]. The ME effect in the SF phase has often being associated with the appearance of a *toroidal moment* $\boldsymbol{T} = \sum_i \mathbf{r_i} \times \mathbf{S_i}$ [25, 26]. However due to the presence of multiple domains in the SF phase (6 domains are predicted, due the 3-fold symmetry breaking), it is unclear whether the ME tensor is purely toroidal (anti-symmetric).

In the Letter, we probe the ME effect in the LF and the in two high-symmetry SF phases ($2'/m$ and $2/m'$) in the ground state of Cr_2O_3 by a set of highly-controlled first-principle calculations — an approach that yields results that are fully consistent with experiments but avoids the domain problem. We demonstrate that the 'large' components of the ME tensor in the SF phase are not intrinsically toroidal. Rather surprisingly, these components are numerically identical to the α_{11} and α_{22} tensor elements in the LF phase, clearly indicating a common origin. We further show that the signs and identical magnitudes of these 'large' ME components can be predicted from the cycloidal spin-current mechanism, which is well

known in multiferroics. Finally, we show that the 'small' ME components in the SF phase arise from two separate mechanisms: a longitudinal response (*e.g.*, α_{33} in the LF phase), which in the ground state is associated with a small longitudinal susceptibility of relativistic origin, whereas it becomes the dominant response at room temperature [27], and a novel chiral ME coupling.

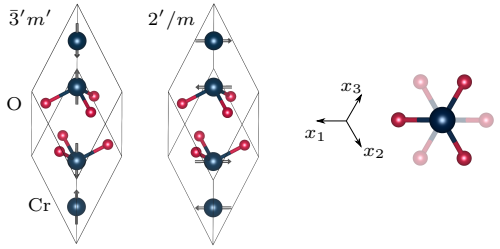

FIG. 1. Structures of Cr_2O_3. Left panel: Rhombohedral primitive cell of Cr_2O_3 with arrows indicating the AFM coupled Cr magnetic moments along z. The magnetic point group is $\bar{3}'m'$. Two 180° domains are possible, linked via time reversal. Middle panel: The spin flop state ($2'/m$ or $2/'m$), with spins aligned in the basal plane, thus breaking the 3-fold symmetry. Right panel: View along z (the half-transparent O atoms belong to the "lower" structural unit). Figures plotted with VESTA [28].

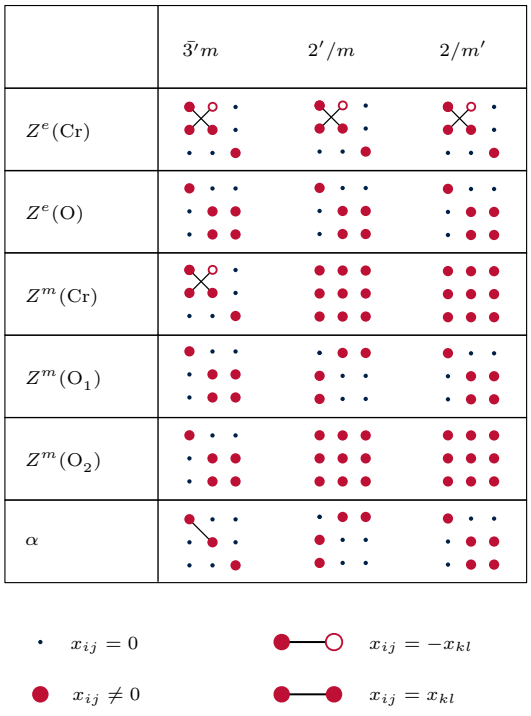

FIG. 2. Tensor forms of the BEC Z^e and magnetic charges Z^m (both based on the atom's site symmetry) and of the overall ME coupling tensor α (based on the point group of the magnetic crystal class).

The ME response of Cr_2O_3 in the LF phase has been the subject of a number of first-principles studies [27, 29–34]. The spin-lattice response $\boldsymbol{\alpha}^{\text{latt}}$ has been shown to be dominant [33], and we therefore focus on this contribution. We take the approach of Ref. [34] and expand the macroscopic response into microscopic quantities as follows:

$$\alpha^{\text{latt}}_{kl} = \frac{\partial P_k}{\partial H_l} = \left(\frac{\partial P_k}{\partial u_i}\right)\left(\frac{\partial u_i \partial u_j}{\partial E}\right)\left(\frac{\partial F_j}{\partial H_l}\right) \qquad (2)$$

with the indices $k, l = 1, 2, 3$ and the composite indices (accounting for three directional dimensions and the number of atoms in the unit cell N) $i, j = 1, \ldots, 3N$. Eq. 2 shows a trilinear relation involving the Born effective charges (BEC) $Z^e_{ki} = \frac{\sigma}{e}\frac{dP_k}{du_i} = -e\frac{dF_i}{d\epsilon_k}$, the inverse of the force-constant (FC) matrix $K^{-1}_{ij} = \frac{\partial u_i}{\partial F_j} = \frac{\partial u_i \partial u_j}{\partial E}$, and the dynamical magnetic charges (MC). The latter can be understood as the magnetic analogue of the BEC and are defined as the derivative of the Hellman-Feynman forces with respect to a magnetic field, $Z^m_{jl} = \frac{\partial F_j}{\partial B_l} = \mu_0^{-1}\frac{\partial F_j}{\partial H_l}$, using $\mathbf{B} = \mu\mathbf{H} \approx \mu_0\mathbf{H}$ and the permeability (vacuum permeability) μ (μ_0) being $\mu \approx \mu_0$ in AFMs.

We calculate the three contributions to Eq. 2 using Density Functional Theory within the local density approximation. We find that spin-orbit coupling (SOC) has a very small effect on the BEC and FC matrix (less than 1 ‰) and we therefore compute these quantities without SOC. This means that our BEC and FC matrix are the same in all three magnetic phases. In contrast, the MC are a SOC induced effect and we compute them using a non-collinear magnetism formalism employing SOC. A Zeeman magnetic field is applied according to Ref. [32] and the change in the ionic forces calculated. It is therefore the changes in the MC which determine the differing form of $\boldsymbol{\alpha}^{\text{latt}}$ in the three magnetic phases. Full details of the DFT calculations, including an analysis of the influence of the choice of exchange-correlation functional are provided in the Supplementary Materials.

Our results for the LF $\bar{3}'m'$ phase were benchmarked against Ref. [34] leading to almost identical results. A full comparison to literature values is given in the Supplementary Material. Table I shows our results for the magnetic charges and for the ME tensor for the LF $\bar{3}'m'$ phase with spins parallel to z, and the two SF phases, $2'/m$ and $2/m'$, with spins *parallel* and *perpendicular* to x, which is also the direction of the surviving 2-fold axis. The tensor forms for both quantities are in good agreement with our group theoretical analysis from Fig. 2. To within $\pm 0.001\,\text{ps}\,\text{m}^{-1}$, which we take to be our computational uncertainty, the ME coupling tensors, are as predicted (bottom row of Fig. 2 and right column of table I).

Because in the $\bar{3}'m'$ phase all improper rotations are coupled to time-reversal symmetry, the MC are of the same form as the BEC. Therefore, those phonon modes that couple to the electric field, *i.e.*, the infrared (IR) active modes, are also the ones that couple to the magnetic field. In the $R\bar{3}c$ space group, the IR active modes are the doubly degenerate E_u modes, which are active

TABLE I. Wyckoff positions, magnetic charges Z^m [$10^{-2}\,\mu_B/\text{Å}$], and the overall ME coupling tensor α [$\text{ps}\,\text{m}^{-1}$] for the LF and to SF phases of Cr_2O_3. The O_1 and O_2 positions in the $\bar{3}'m'$ phase are related by a 3-fold rotation and the Z^m given in the following table for comparison with the SF cases.

Phase	w(Cr)	w(O_1)	w(O_2)	Z^m(Cr)	Z^m(O_1)	Z^m(O_2)	α
$\bar{3}'m'$	$4c$	$6e$	$6e$	$\begin{pmatrix} 2.4 & 5.6 & 0.0 \\ -5.6 & 2.4 & 0.0 \\ 0.0 & 0.0 & 0.0 \end{pmatrix}$	$\begin{pmatrix} -2.8 & 0.0 & 0.0 \\ 0.0 & -0.5 & -0.0 \\ 0.0 & -2.7 & -0.0 \end{pmatrix}$	$\begin{pmatrix} -1.1 & 1.0 & 0.0 \\ 1.0 & -2.2 & 0.0 \\ 2.3 & 1.4 & 0.0 \end{pmatrix}$	$\begin{pmatrix} 0.310 & 0.000 & -0.001 \\ 0.000 & 0.310 & 0.000 \\ 0.000 & 0.000 & 0.005 \end{pmatrix}$
$2'/m$	$8f$	$4e$	$8f$	$\begin{pmatrix} 0.0 & -0.1 & -2.3 \\ 0.0 & 0.0 & 5.6 \\ 0.1 & 18.9 & 0.0 \end{pmatrix}$	$\begin{pmatrix} 0.0 & -1.5 & 3.0 \\ -0.3 & 0.0 & 0.0 \\ -0.1 & 0.0 & 0.0 \end{pmatrix}$	$\begin{pmatrix} 0.3 & 0.8 & 0.8 \\ 0.2 & -1.4 & -1.2 \\ -0.1 & -0.1 & -2.2 \end{pmatrix}$	$\begin{pmatrix} -0.001 & -0.012 & -0.309 \\ 0.001 & -0.001 & 0.000 \\ 0.019 & 0.000 & 0.000 \end{pmatrix}$
$2/m'$	$8f$	$4e$	$8f$	$\begin{pmatrix} -0.1 & 0.0 & -5.6 \\ 0.0 & 0.0 & -2.3 \\ -18.8 & 0.2 & 0.0 \end{pmatrix}$	$\begin{pmatrix} 1.7 & 0.0 & 0.0 \\ 0.0 & -0.3 & 0.1 \\ 0.0 & -0.1 & 2.5 \end{pmatrix}$	$\begin{pmatrix} -0.7 & 0.3 & -1.2 \\ 1.3 & 0.2 & 2.2 \\ -0.1 & -0.1 & -1.3 \end{pmatrix}$	$\begin{pmatrix} -0.012 & 0.000 & 0.000 \\ 0.000 & -0.002 & -0.309 \\ 0.000 & 0.019 & 0.001 \end{pmatrix}$

in the xy plane, and the singly degenerate A_{2u} modes, active along z. Not including the acoustic modes, the Γ-centred IR active modes are therefore

$$\Gamma^{\text{IR}} = 4E_u + 2A_{2u}. \tag{3}$$

From a mode decomposition of the BEC and the MC, we observe changes in the magneto-active response when x and y are no longer equivalent. The degeneracy of the IR active E_u modes is removed, and other modes become magneto-active in x, y, or z. We also find that the exceptionally large component in the Z^m(Cr) (the 32 and 31 component in the $2'/m$ and $2/m'$ phase, respectively) maps onto magneto-active modes that are mutually exclusive to the IR active ones. That value has therefore no effect on the coupling tensor. Even though the magnetic charge tensors are quite dissimilar, this leads to the rather surprising similarity of the coupling tensors. The full mode decomposition of the BEC and the MC for the LF phase is given in the Supplementary Material.

On this basis, we make the following important observations. Firstly, the ME tensor α is *not* what one would expect from a toroidal moment. There is clearly a toroidal (antisymmetric) component, but this is identical in magnitude to the traceless symmetric component. This should not be particularly surprising, since the toroidal mechanism $\mathbf{P} = \boldsymbol{T} \times \mathbf{H}$ does not capture the large difference between the longitudinal and transverse susceptibilities. Secondly, the magnitudes of the 'large' elements of the ME tensor is the same (within error) in the two SF phases *and* in the LF phase. In fact, all these large ME responses can be approximated by the following compact expression:

$$\boldsymbol{\alpha}^{\text{latt}} \approx 0.31\,\text{ps}\,\text{m}^{-1} \begin{pmatrix} \hat{m}_z & 0 & -\hat{m}_x \\ 0 & \hat{m}_z & -\hat{m}_y \\ 0 & 0 & 0 \end{pmatrix} \tag{4}$$

where $\hat{m}_x$, $\hat{m}_y$ and $\hat{m}_z$ are the components of a unit vector parallel to the spin on the Cr($4c$) atom at Wyckoff position 0.1590. A clue as to the origin of this tensor form is the fact the all these components correspond to a *transverse* spin response in the plane containing both the spins and z, so that the rotated spins under the action of the magnetic field can be thought as forming a segment of a cycloid. Here below, we show that the tensor form in Eq. 4 is exactly the one predicted from the spin current [35] or inverse Dzyaloshinsky-Moriya (DM) [36] mechanisms, which are well known in the context of multiferroics. We write the transverse response of the magnetisation $\mathbf{m}_i$ on Cr site i as

$$\begin{aligned} \Delta\mathbf{m}_i &= \chi^T \frac{\mathbf{m}_i \times (\mathbf{H} \times \mathbf{m}_i)}{m^2} \\ &= \chi^T \left(\mathbf{H} - \frac{\mathbf{m}_i\,(\mathbf{H} \cdot \mathbf{m}_i)}{m^2} \right) \end{aligned} \tag{5}$$

where χ^T is the transverse susceptibility. The inverse DM polarisation is:

$$\begin{aligned} \mathbf{P} &= \mu \mathbf{r}_{12} \times (\mathbf{m}_1 \times \mathbf{m}_2) = 2\mu\chi^T \mathbf{r}_{12} \times (\mathbf{m} \times \mathbf{H}) \\ &= 2\mu\chi^T \left(\mathbf{m}\,(\mathbf{H} \cdot \mathbf{r}_{12}) - \mathbf{H}\,(\mathbf{m} \cdot \mathbf{r}_{12}) \right) \end{aligned} \tag{6}$$

where μ is a coupling constant and, in the case of Cr_2O_3, $\mathbf{r}_{12} \parallel c$. With this, the ME tensor takes the form:

$$\begin{aligned} \boldsymbol{\alpha} &= 2\mu\chi^T \left(\mathbf{m} \otimes \mathbf{r}_{12} - \mathbf{m} \cdot \mathbf{r}_{12} \mathbb{1} \right) \\ &= -2\mu\chi^T \begin{pmatrix} m_z & 0 & -m_x \\ 0 & m_z & -m_y \\ 0 & 0 & 0 \end{pmatrix} \end{aligned} \tag{7}$$

where $\otimes$ is the outer (tensor) product and $\mathbb{1}$ is the unit tensor. Eq. 7 and Eq. 4 have exactly the same form, including the non-trivial sign of the tensor elements.

In all phases, the ME tensor latt has a small longitudinal term (i.e., with the field H parallel to the spins) of magnitude $0.005\,\text{ps}\,\text{m}^{-1}$ ($0.019\,\text{ps}\,\text{m}^{-1}$) for the LF (SF) phase(s), which generates $P \parallel z$ in all cases. In the ground state, this is associated with a small longitudinal susceptibility of relativistic origin, while at finite temperatures, the symmetric Heisenberg exchange makes this term become the dominant contribution to α in the LF phase, as shown in Ref. [27].

Considerably more interesting is the additional *in-plane transverse* term of magnitude $-0.012\,\mathrm{ps\,m^{-1}}$, which is only present in the SF phases. Here, the field H lies in the xy plane perpendicular to the spins and generates $P \parallel x$, i.e., to the surviving 2-fold axis of the monoclinic structure. Phenomenologically, this term is associated with a *fifth order* invariant of the form $(m_x^2 - m_y^2)A_x - 2m_x m_y A_y$ where $\mathbf{A} = (m_y H_x - m_x H_y)\mathbf{P}$ transforms as an axial (parity-even) vector. In the remainder, we show that this term is due to the breaking of axial symmetry upon SF magnetic ordering, coupled with the breaking of chiral symmetry upon application of a magnetic field in the in-plane transverse direction.

As we already mentioned, SF magnetic ordering breaks the 3-fold symmetry. Consequently, the *crystallographic* symmetry is also lowered, due to coupling of the staggered magnetisation with a structural order parameter, which has the transformation properties of an axial vector $\mathbf{A}$. Minimising the Landau free energy with respect to $\mathbf{A}$ in the usual way, one obtains:

$$\begin{aligned} A_x &= \lambda(m_x^2 - m_y^2) \\ A_y &= -\lambda(m_x m_y) \end{aligned} \tag{8}$$

where λ is a (small) magneto-elastic coupling constant. It is noteworthy that $A_y = 0$ in both of the SF phases we considered, so $\mathbf{A}$ is directed along x. Upon application of a magnetic field in the in-plane transverse direction, the rotated spins can be thought as forming a segment of a helix, which has the distinct chirality $\mathbf{r}_{12} \cdot (\mathbf{m}_1 \times \mathbf{m}_2)$. In analogy to the ferroaxial multiferroic mechanism [37, 38], we can therefore write the following phenomenological polarisation:

$$\begin{aligned} P_x &= \mu\lambda(m_x^2 - m_y^2)\, \mathbf{r}_{12} \cdot (\mathbf{m}_1 \times \mathbf{m}_2) \\ &= 2\mu\chi^T\lambda(m_x^2 - m_y^2)\, \mathbf{r}_{12} \cdot (\mathbf{m} \times \mathbf{H}) \\ &= 2\mu\chi^T\lambda(m_x^2 - m_y^2)\ (\mathbf{r}_{12} \times \mathbf{m}) \cdot \mathbf{H} \\ P_y &= 0 \end{aligned} \tag{9}$$

yielding

$$\boldsymbol{\alpha} = 2\mu\chi^T\lambda(m_x^2 - m_y^2)\hat{\mathbf{x}} \otimes (\mathbf{r}_{12} \times \mathbf{m}) \tag{10}$$

where $\hat{\mathbf{x}}$ is a unit vector along x. Since $(\mathbf{r}_{12} \times \mathbf{m}) = (-m_y, m_x, 0)$, the ME tensor has the desired form

$$\boldsymbol{\alpha} = -2\mu\chi^T\lambda m^2 \begin{pmatrix} m_y & m_x & 0 \\ 0 & 0 & 0 \\ 0 & 0 & 0 \end{pmatrix} \tag{11}$$

which corresponds to the first-principle result. By comparing Eq. 11 with Eq. 7, one can understand why the former, containing the small parameter λ, is considerably smaller than the latter.

In summary, we have computed the magneto-electric tensor of Cr_2O_3 in both low-field and high-field (spin flop) phases by means of highly-controlled first-principle calculations. We find that the ME tensor is not primarily toroidal, as previously speculated. Instead, its approximate form can be well predicted phenomenologically using the spin-current model, which is well known in multiferroics. There are two additional small components: the first is a longitudinal component known from previous studies of the low-field phase, while the second arises from a novel chiral mechanism, which is akin to the ferroaxial mechanisms in multiferroics.

The work done at the University of Oxford was funded by EPSRC grants, number EP/J003557/1, entitled "New Concepts in Multiferroics and Magnetoelectrics" and number EP/M020517/1, entitled "Oxford Quantum Materials Platform Grant", the Scatcherd European Scholarship (NT), and The Royal Society (JRY). This work used the ARCHER UK National Supercomputing Service (http://www.archer.ac.uk), for which access was obtained via the UKCP consortium and funded by EPSRC grant ref EP/K013564/1. We are also grateful for many valuable discussions with M. Ye and D. Vanderbilt.

* natalie.tillack@materials.ox.ac.uk

[1] H. Schmid, Ferroelectrics **162**, 317 (1994).
[2] M. Fiebig, Journal of Physics D: Applied Physics **38**, R123 (2005).
[3] S.-W. Cheong and M. Mostovoy, Nature Materials **6**, 13 (2007).
[4] J. F. Scott, Journal of Materials Chemistry **22**, 4567 (2012).
[5] W. Eerenstein, N. D. Mathur, and J. F. Scott, Nature **442**, 759 (2006).
[6] M. Fiebig and N. A. Spaldin, The European Physical Journal B **71**, 293 (2009).
[7] P. Borisov, A. Hochstrat, X. Chen, W. Kleemann, and C. Binek, Physical Review Letters **94**, 117203 (2005).
[8] P. Borisov, A. Hochstrat, V. V. Shvartsman, and W. Kleemann, The Review of Scientific Instruments **78**, 106105 (2007).
[9] L. D. Landau and E. M. Lifshitz, *Electrodynamics of Continuous Media* (Oxford Pergamon Press, Oxford, 1960).
[10] I. Dzyaloshinsky, Journal of Physics and Chemistry of Solids **4**, 241 (1958).
[11] I. E. Dzyaloshinskii, Sov. Phys. JETP **10**, 628 (1960).
[12] D. N. Astrov, Sov. Phys. JETP **11**, 708 (1960).
[13] D. N. Astrov, Sov. Phys. JETP **13**, 729 (1961).
[14] V. J. Folen, G. T. Rado, and E. W. Stalder, Physical Review Letters **6**, 607 (1961).
[15] G. T. Rado, Physical Review **128**, 2546 (1962).
[16] G. T. Rado and V. J. Folen, Journal of Applied Physics **33**, 1126 (1962).
[17] M. Street, W. Echtenkamp, T. Komesu, S. Cao, P. A. Dowben, and C. Binek, Applied Physics Letters **104**, 222402 (2014).
[18] H. Wiegelmann, a. G. M. Jansen, P. Wyder, J.-P. Rivera, and H. Schmid, Ferroelectrics **162**, 141 (1994).
[19] A. S. Borovnik-Romanov and H. Grimmer, in *Interna-*

tional Tables for Crystallography, Vol. D (John Wiley and Sons, Inc, 2006) Chap. 1.5, pp. 105–149.
[20] J. W. Allen, Physical Review B **7**, 4915 (1973).
[21] M. R. J. Gibbs, *Modern Trends in Magnetostriction Study and Application* (Springer Science & Business Media, 2001) p. 242.
[22] E. Kita, K. Siratori, and A. Tasaki, Journal of Applied Physics **50**, 7748 (1979).
[23] A. Scaramucci, E. Bousquet, M. Fechner, M. Mostovoy, and N. A. Spaldin, Physical Review Letters **109**, 197203 (2012).
[24] J. Ohtani and K. Kohn, J. Phys. Soc. Jpn. **53**, 3744 (1984).
[25] Y. F. Popov, A. M. Kadomtseva, D. V. Belov, and G. P. Vorob, Journal of Experimental and Theoretical Physics Letters **69**, 330 (1999).
[26] N. A. Spaldin, M. Fiebig, and M. Mostovoy, Journal of Physics: Condensed Matter **20**, 434203 (2008).
[27] M. Mostovoy, A. Scaramucci, N. A. Spaldin, and K. Delaney, Physical Review Letters **105**, 087202 (2010).
[28] K. Momma and F. Izumi, Journal of Applied Crystallography **44**, 1272 (2011).
[29] J. Íñiguez, Physical Review Letters **101**, 12 (2008).
[30] S. Coh, D. Vanderbilt, A. Malashevich, and I. Souza, Physical Review B **83**, 85108 (2011).
[31] E. Bousquet and N. A. Spaldin, Physical Review Letters **107**, 1 (2011).
[32] E. Bousquet, N. A. Spaldin, and K. Delaney, Physical Review Letters **106**, 1 (2011).
[33] A. Malashevich, S. Coh, I. Souza, and D. Vanderbilt, Physical Review B **86**, 1 (2012).
[34] M. Ye and D. Vanderbilt, Physical Review B **89**, 064301 (2014).
[35] H. Katsura, N. Nagaosa, and A. V. Balatsky, Physical Review Letters **95**, 057205 (2005).
[36] M. Mostovoy, Physical Review Letters **96**, 067601 (2006).
[37] R. D. Johnson, S. Nair, L. C. Chapon, a. Bombardi, C. Vecchini, D. Prabhakaran, a. T. Boothroyd, and P. G. Radaelli, Physical Review Letters **107**, 2 (2011).
[38] R. D. Johnson, L. C. Chapon, D. D. Khalyavin, P. Manuel, P. G. Radaelli, and C. Martin, Physical Review Letters **108**, 2 (2012).

Supplementary Material for *Ab Initio* Cycloidal and Chiral Magnetoelectric Responses in Cr_2O_3

Natalie Tillack* and Jonathan R. Yates
Department of Materials, University of Oxford, Oxford, OX1 3PH, United Kingdom

Paolo G. Radaelli
Department of Physics, University of Oxford, Oxford, OX1 3PU, United Kingdom

(Dated: February 26, 2016)

The Supplementary Material consists of two parts: It gives the computational details and illustrates the choice of DFT parameters, as well as a comparison to literature values of magnetoelectric (ME) and ground state properties.

COMPUTATIONAL DETAILS

We employed the DFT code VASP [1] using projector augmented wave (PAW) potentials [2]. For the Cr atoms, we treated the $3d$ and $4s$ electrons as valence, for O the $2s$ and $2p$ electrons. The plane wave basis set was cut off for energies above 550 eV and a $4\times4\times4$ Monkhorst-Pack grid centred around Γ [3] guarantee convergence of the total energy and magnetisation of 0.1 meV and $10^{-5}\,\mu_B$, respectively. We employed the local density approximation (LDA) and the generalised gradient approximation (GGA) with its implementation by Perdew, Burke, and Ernzerhof (PBE) [4]. Blöchl's corrections for the tetrahedron smearing method were employed with a broadening width of 0.05 eV. The structures were relaxed with the conjugated gradient algorithm; a tight convergence criterion of $5\times10^{-6}\,\mathrm{eV\,Å^{-2}}$ had to be chosen to account for the sensitive response of the forces to the magnetic field. No symmetry constraints were used for the calculations.

The BEC were computed using both the $^{\partial\mathbf{P}}/_{\partial\mathbf{u}}$ and the $^{\partial\mathbf{F}}/_{\partial\boldsymbol{\epsilon}}$ implementation to verify the numerical accuracy of the calculations. Both finite differences and density functional perturbation theory were tested and led to similar results when computing the FC matrix. The BEC and the FC matrix were calculated for the $\bar{3}'m'$ ground state treating spins collinearly and as spinors, within the collinear and spinor formalism, leading to identical results to the fourth decimal place. Allowing for noncollinear magnetism in Cr_2O_3 did not have a significant influence on the BEC and the FC matrix, which was to be expected, as both couple to the lattice and SOC in Cr_2O_3 is small. We thus confirmed that collinear calculations are sufficient for the computation of the FC matrix and the BEC. For the computation of the magnetic charges, spin-orbit coupling (SOC) was included, a Zeeman magnetic field applied according to [5], and the Hellman-Feynman forces on each atom computed. By using the same BEC and FC matrix results for all three magnetic phases, we isolated the influence of the magnetic charges.

COMPARISON TO LITERATURE

The equilibrium parameters of the $\bar{3}'m'$ phase of Cr_2O_3 were calculated for both xc functionals and benchmarked against literature values, table I. The differences are well known in DFT: An over- (under-) binding when using LDA (PBE), the magnetic moment increasing when going from LDA to PBE, and the electronic band gap underestimated by both functionals.

TABLE I. Structural, electronic, and magnetic properties of Cr_2O_3 using different xc functionals and benchmarked against literature values.

Details	a_{Lat} [Å]	M_{Cr} [μ_B]	E_{Gap} [eV]
LDA	5.26	2.2	0.8
PBE	5.42	2.7	1.7
LDA+U, Ref. [6]	5.37	2.8	2.8
LDA, Ref. [7]	5.32	2.0	1.3
SQUID, Ref. [8]	5.36	2.65 / 2.31	

For simplicity, because it provides a more stable implementation with noncollinear magnetism than the GGA functionals, and because it leads to a reasonably good description of the ground state, the results given in the main text are based on our LDA calculations.

We did however repeat the calculations for the ME coupling tensor of the LF $\bar{3}'m'$ phase using PBE and compared to the results in Ref. [9] leading to almost identical results, table II. The results are given in the basis of the IR active phonon modes, which for Cr_2O_3 are the four doubly degenerate transverse E_u and two singly degenerate longitudinal A_{2u} modes. We noticed that the differences between GGA and LDA functionals in the strength of the ME coupling are mainly attributed to the different lattice constant that both functionals predict.

From the mode decomposition of the BEC and the magnetic charges in the two SF phases, we observe changes in the magneto-active response due to x and y no longer being equivalent. The degeneracy of the IR

TABLE II. Comparison of the mode decomposed Born effective charges (in e), magnetic charges (in $10^{-2}\,\mu_B/\text{Å}$), the overall ME coupling tensor (in $\text{ps}\,\text{m}^{-1}$), and the respective eigenvalues of the FC matrix C_n (in $\text{eV}/\text{Å}^2$) for the $\bar{3}'m'$ phase of Cr_2O_3 compared to Ref. [9]. The PBE functional was used in both cases.

Mode	PBE				PBE, Ref. [9]			
	Z^e	Z^m	C	α	Z^e	Z^m	C	α
${E_u}^1$	6.8	9.5	29	0.263	7.1	10.6	31	0.290
${E_u}^2$	3.8	14.9	19	0.361	3.7	16.1	20	0.356
${E_u}^3$	0.2	-3.7	15	-0.005	0.4	-4.0	16	-0.012
${E_u}^4$	0.8	-0.0	10	0.000	0.6	-0.8	10	-0.005
All $\perp$				0.618				0.629
${A_{2u}}^1$	8.6	0.1	21	0.003	8.5	0.1	23	0.002
${A_{2u}}^2$	1.0	0.0	10	0.001	1.2	0.0	11	0.000
All $\parallel$				0.004				0.003

active E_u modes is removed, and other modes become magneto-active in x, y, or z. We also find that the exceptionally large component in the Z^m(Cr) (the 32 and 31 component in the $2'/m$ and $2/m'$ phase, respectively; results given in the main text) maps onto magneto-active modes that are mutually exclusive to the IR active ones. That value has therefore no effect on the coupling tensor, explaining why – despite the magnetic charge tensors being quite different in the LF and SF cases – in all three coupling tensors related elements have similar numerical values.

* natalie.tillack@materials.ox.ac.uk

[1] G. Kresse and J. Furthmüller, Physical Review B - Condensed Matter and Materials Physics B, Condensed matter **54**, 11169 (1996).

[2] P. E. Blöchl, Physical Review B **50**, 17953 (1994).

[3] H. J. Monkhorst and J. D. Pack, Physical Review B **13**, 5188 (1976).

[4] J. Perdew, K. Burke, and M. Ernzerhof, Physical review letters **77**, 3865 (1996).

[5] E. Bousquet and N. A. Spaldin, Physical Review Letters **107**, 1 (2011).

[6] N. J. Mosey, P. Liao, and E. A. Carter, The Journal of chemical physics **129**, 014103 (2008).

[7] S. Coh, D. Vanderbilt, A. Malashevich, and I. Souza, Physical Review B **83**, 85108 (2011).

[8] A. H. Hill, A. Harrison, C. Dickinson, W. Zhou, and W. Kockelmann, Microporous and Mesoporous Materials **130**, 280 (2010).

[9] M. Ye and D. Vanderbilt, Physical Review B **89**, 064301 (2014).